An Accurate Multiobjective Optimization Strategy for Surface-Mounted Permanent-Magnet Machines Based on Nonlinear Finite-Permeability Subdomain Model

Che Sun[1], Youtong Fang[1,2], and Pierre-Daniel Pfister[1,2]

[1]College of Electrical Engineering, Zhejiang University, Hangzhou 310027, China
[2]Zhejiang Provincial Key Laboratory of Electrical Machine Systems, Zhejiang University, Hangzhou 310027, China

This article presents an accurate multiobjective optimization strategy for surface-mounted permanent-magnet machines (SMPMMs) by combining a nonlinear finite-permeability subdomain model (FPSM) with the nondominated sorting genetic algorithm II (NSGA-II). The nonlinear FPSM is developed by introducing a nonlinear iterative algorithm (NIA) to consider the magnetic saturation of soft magnetic materials and applied to SMPMMs. For the NIA, two iterative solving methods (ISMs), namely bisection and relaxation methods (RMs), are compared for the convergence speeds through statistical analysis of 500 designs. This analysis shows that the RM is the best in terms of computation time. When the relaxation coefficient equals to 1, the number of iterations comes down to 2 for this specific machine with the given allowable error. The electromagnetic performances of one optimal case are validated by finite-element models (FEMs) to demonstrate the effectiveness of the presented optimization strategy. The strategy proposed in this article can help designers to find the optimal designs for SMPMMs.

***Index Terms*— Finite-permeability subdomain models (FPSMs), magnetic saturation, nondominated sorting genetic algorithm II (NSGA-II), statistical analysis, surface-mounted permanent-magnet machine (SMPMM).**

I. Introduction

PERMANENT-MAGNET (PM) machines are widely used in industrial manufacture and household appliances due to their high efficiency and torque density. A fast and accurate modeling approach is essential for motor design and optimization.

Finite-element models (FEMs) have proven to be a highly effective technique for designing PM machines because they can consider magnetic saturation and complex geometries. However, the design process using FEM is too time-consuming. Subdomain (SD) models, as a favorable alternative to FEM, have faster calculation speed [1], [2]. However, the traditional SD models assume that the permeability of iron parts is infinite, and the magnetic saturation effect of ferromagnetic materials is hence ignored. Two different finite-permeability subdomain models (FPSMs) have been proposed to consider the magnetic saturation effect. The first one gives the general solutions of Maxwell's equations for every SD by considering nonhomogeneous Neumann boundary conditions and both θ-edge and r-edge interface conditions [3]. The other type of FPSM divides the machine into an arbitrary number of homogeneous or nonhomogeneous layers where the permeability in the stator or rotor slotting is represented as a Fourier series along the direction of permeability variation [4].

Many studies on the optimal design of electric machines are primarily based on FEM [5], [6], [7], which is very time-consuming because of the many iterations needed during the optimization process. Few studies combine the nonlinear FPSM with an optimization algorithm to accelerate the optimization process. Zhao et al. [8] combined the second type of FPSM with nondominated sorting genetic algorithm II (NSGA-II) to optimize Vernier machines. The first type of FPSM is more accurate than the second type of FPSM when studying magnetic saturation and optimizing parameters [9]. However, to our knowledge, the first type of FPSM has not been combined with any optimization algorithm.

In this article, an accurate multiobjective optimization strategy for surface-mounted PM machines (SMPMMs) is presented, which is based on combining the first type of FPSM with NSGA-II. A nonlinear iterative algorithm (NIA) is introduced to consider the magnetic saturation effect. Based on statistical analysis, this article compares the convergence speed of two different iterative solving methods (ISMs): the bisection method (BM) and the relaxation method (RM). To our knowledge, this is the first time these two ISMs are compared for the first type of FPSM, which can help designers find the best ISM for them and accelerate the process of obtaining the optimal designs. The optimal objectives in this study are average torque, torque ripple, and PM usage. Finally, an optimal case is selected from the Pareto front and validated by FEM.

II. Studied SMPMM and Nonlinear FPSM

A. Studied SMPMM

The structure of the studied SMPMM is shown in Fig. 1, and the fixed parameters during optimization are given in Table I. As shown in Fig. 1, the studied machine is divided into six types of SDs. SD I to VI represent the rotor yoke, the PMs, the air gap, the stator slots, the stator teeth, and the stator yoke, respectively. The radii R_1, R_2, R_3, R_4, R_5, and R_6 are the

Manuscript received 19 March 2024; revised 28 May 2024; accepted 7 June 2024. Date of publication 12 June 2024; date of current version 27 August 2024. Corresponding author: P.-D. Pfister (e-mail: pierredaniel.pfister.public@gmail.com).

Color versions of one or more figures in this article are available at https://doi.org/10.1109/TMAG.2024.3413541.

Digital Object Identifier 10.1109/TMAG.2024.3413541

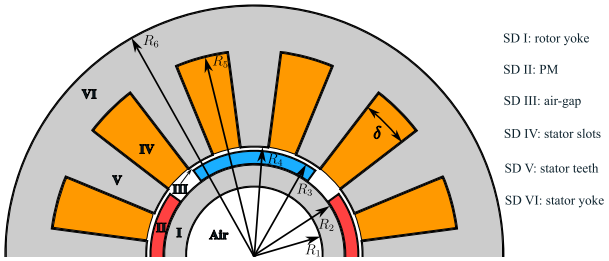

Fig. 1. Structure of the studied SMPMM.

TABLE I
FIXED PARAMETERS DURING OPTIMIZATION

Parameter	Value
Number of stator slots Q_s	12
Number of pole pairs p	2
Stator outer radius R_6	53 mm
Air-gap length g	0.8 mm
PM remanence B_R	1.45 T
Active length l_a	100 mm
Current density J_{max}	8 A/mm^2

rotor inner radius, the PM inner radius, the PM outer radius, the air gap outer radius, the slot outer radius, and the stator outer radius, respectively. The stator opening angle is marked as δ. The analytical model in this article is formulated in the 2-D polar coordinate system based on the assumptions shown in [9]. However, contrary to [9], the permeability of the rotor yoke is finite, and the magnetic saturation effect of this SD is considered.

B. Introduction of FPSM

The six types of SDs are shown in Fig. 2. The governing equations of magnetic vector potential (MVP) derived from the magnetostatic Maxwell's equations are formulated for different SDs based on the material properties of each SD. The general solution of MVP for each SD is obtained by using the Fourier series and the separation variables in polar coordinates. The general solutions of MVP for SD II to VI are given in [9] and [10]. In this article, the magnetic field of the rotor yoke (SD I) is considered. The general solution of MVP in the rotor yoke is given by

$$\begin{aligned} A_{zI} = {} & A_{10} \cdot \ln\left(\frac{r}{R_1}\right) \\ & + \sum_{n=1}^{\infty} A_{2n} \cdot \left[\left(\frac{r}{R_1}\right)^n - \left(\frac{r}{R_1}\right)^{-n}\right] \cdot \sin(n\theta) \\ & + \sum_{n=1}^{\infty} A_{3n} \cdot \left[\left(\frac{r}{R_1}\right)^n - \left(\frac{r}{R_1}\right)^{-n}\right] \cdot \cos(n\theta) \end{aligned} \quad (1)$$

where A_{10}, A_{2n}, and A_{3n} are SD I's integration constants.

The boundary conditions (BCs) are used to connect these general solutions of MVP to build a linear system. The six types of SDs in this SMPMM can be divided into two types: 1) periodic SDs, such as SD I, II, III, and VI; and 2) nonperiodic SDs, such as SD IV and V. There are two types of BCs considered in this model. One BC type is over angle intervals for a given radius (θ-edges), and the other is

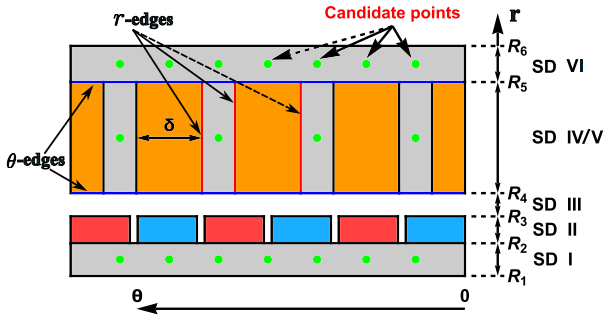

Fig. 2. Representation of the different SDs.

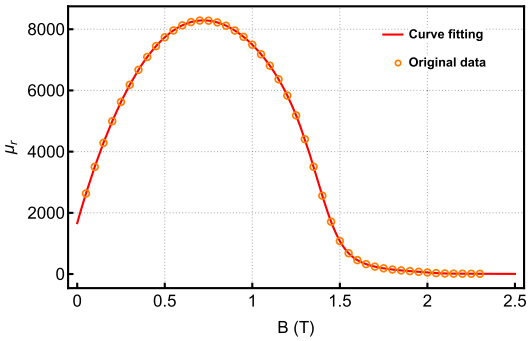

Fig. 3. Relative permeability versus magnetic flux density curve of M19 steel.

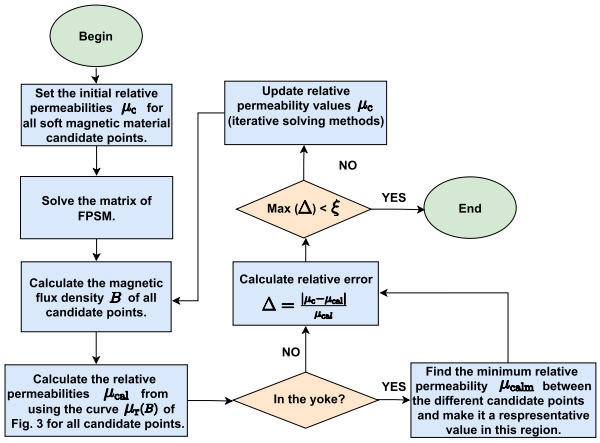

Fig. 4. Structure of the nonlinear algorithmic solution.

over radius intervals for given angles (r-edges) [3]. These two types of BCs are shown in Fig. 2. Both θ-edges and r-edges BCs are considered in nonperiodic SDs, but only θ-edges BCs need to be considered in periodic SDs. All BCs are given in [3] and [9]. Finally, the constants for each SD are determined by solving the linear system obtained from the BCs.

C. Nonlinear Iterative Algorithm

The nonlinear ferromagnetic material M-19 steel is used in SD I, V, and VI. The $\mu_r - B$ curve is shown in Fig. 3.

The flowchart of the NIA is shown in Fig. 4. Some candidate points (CPs) are selected (Fig. 2) to consider the nonlinearity. First, the relative permeabilities of all soft magnetic material CPs are set to an initial value μ_c. Then, the magnetic flux

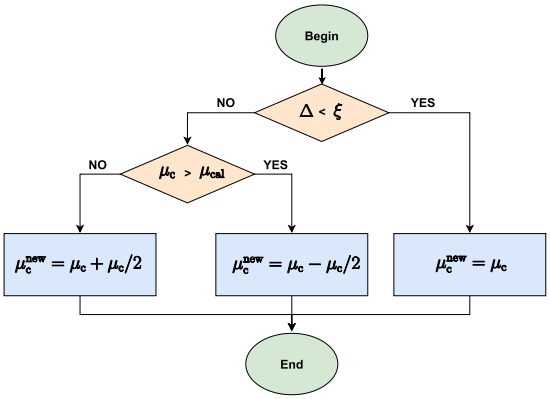

Fig. 5. Bisection method.

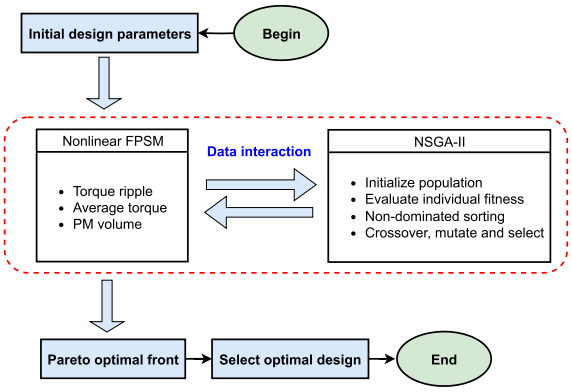

Fig. 6. Flowchart of the proposed multiobjective optimization strategy.

density of each CP is obtained by solving the matrix of the linear system, and the calculated relative permeability for all CPs (μ_{cal}) is obtained based on the curve $\mu_r(B)$ shown in Fig. 3. The calculated relative permeability in the SDs I and VI requires selecting the minimum value μ_{calm} among all CPs in each SD as the representative value for the whole SD. Next, all CPs' relative permeability is iteratively updated all using the ISM. The BM, shown in Fig. 5, is used as the ISM to take the nonlinearity into account. When the relative errors Δ are smaller than the allowable errors ξ, the algorithm is finished.

III. Optimization Process

There are many objectives during the motor design, such as high average torque and low torque ripple. However, these objectives are usually in conflict with one another. Many algorithms are developed to find the optimal design, such as genetic algorithm, particle swarm optimization, and NSGA-II, that can be used for multiobjective optimization. In this article, NSGA-II is adopted as an optimization algorithm and combined with the nonlinear FPSM mentioned above to search for the optimal design for SMPMMs. The flowchart of the proposed multiobjective optimization strategy is illustrated in Fig. 6, and the average torque, torque ripple, and PM volume represent the individual fitness.

The fixed parameters and the design variables with the corresponding range during optimization are provided in Tables I and II, respectively. We aim to maximize the

TABLE II
Value Range of Design Parameters During Optimization

Parameter	Range
Thickness of rotor yoke ($R_2 - R_1$)	3-15 mm
Thickness of PM ($R_3 - R_2$)	1-10 mm
Stator tooth length ($R_5 - R_4$)	5-30 mm
Thickness of stator yoke ($R_6 - R_5$)	3-15 mm
Slot opening angle δ	10-25°
PM pole arc ratio η	0.5-1

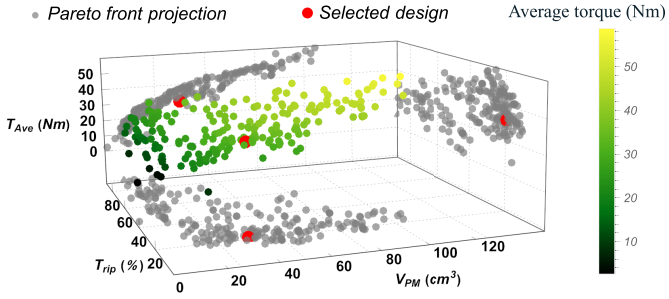

Fig. 7. Three-dimensional Pareto front of the optimized SMPMMs with corresponding 2-D projections.

TABLE III
Design Parameters of Optimization Cases

Parameters	Value	Unit
Rotor inner radius R_1	13	mm
PM inner radius R_2	19	mm
PM outer radius R_3	22.1	mm
Air gap outer radius R_4	22.9	mm
Slot outer radius R_5	46	mm
PM pole arc ratio η	0.86	
Slot opening angle δ	19.4	degree

output average torque T_{ave} in a constrained motor volume and minimize the torque ripple T_{ripple} to reduce the vibration and noise. We also aim to reduce the PM volume V_{PM} to lower manufacturing costs. Therefore, the optimization objectives are set as average torque (T_{ave}), torque ripple (T_{rip}), and PM volume (V_{PM}), and the objective functions and constraint are listed as follows:

$$\begin{cases} \text{Functions: } \left[\text{Max}(T_{\text{ave}}), \text{Min}\left(T_{\text{rip}}\right), \text{Min}(V_{\text{PM}})\right] \\ \text{Constraint: } R_1 > 0. \end{cases} \tag{2}$$

The maximum number of generations is set at 200, and the population for each generation is set at 20. The optimization results with a clear 3-D Pareto front and corresponding 2-D projections are presented in Fig. 7. An optimal case on the Pareto front is selected for validation, and the parameters are shown in Table III. The time to solve the matrix generated by the FPSM once is about 0.4 s. For each calculation point, multiple rotor positions need to be calculated, and each rotor position requires several matrix calculations.

IV. FEM Validation

In order to validate the accuracy of the proposed optimization strategy, the electromagnetic parameters calculated by nonlinear FPSM for the selected optimal case, such as magnetic flux density, electromagnetic torque, and cogging

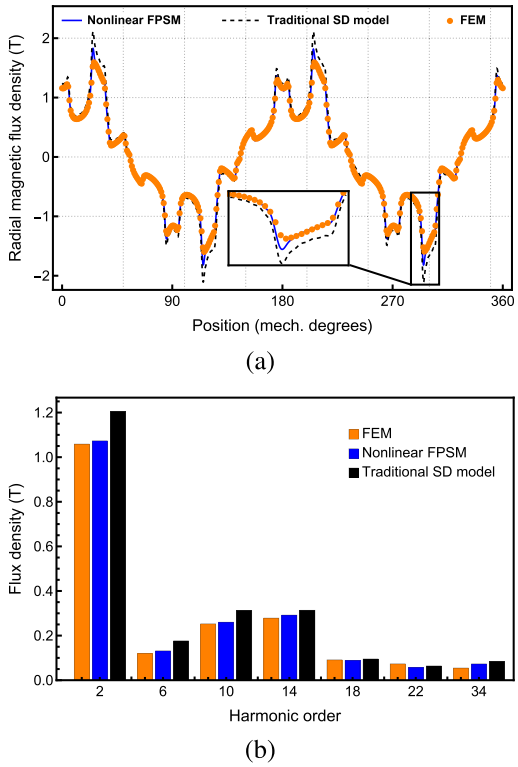

Fig. 8. On-load radial magnetic flux density in the middle air gap of an optimal case. (a) Flux density distribution. (b) Harmonic spectrum.

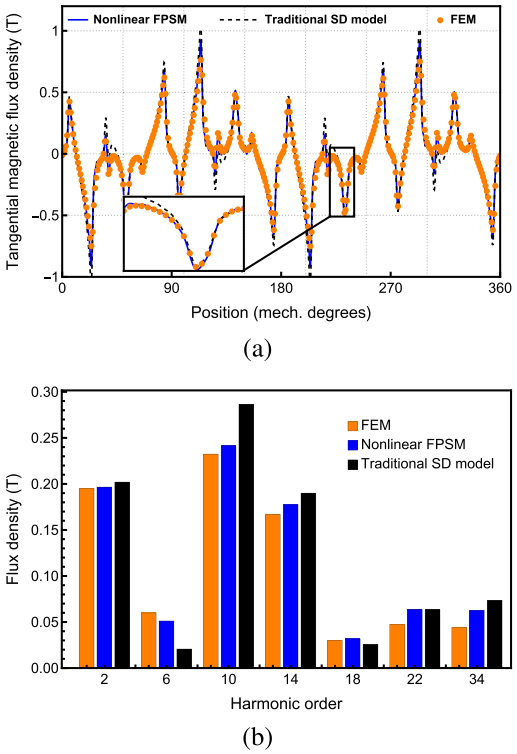

Fig. 9. On-load tangential magnetic flux density in the middle air gap of an optimal case. (a) Flux density distribution. (b) Harmonic spectrum.

torque, are compared with FEM and with the traditional SD model.

The on-load radial and tangential magnetic flux density distribution in the middle of the air gap and the corresponding harmonic spectrum are shown in Figs. 8 and 9, respectively. The relative errors of radial flux density for the nonlinear FPSM and traditional SD model are 3.5% and 12.6%, respectively. The electromagnetic torque calculated by the nonlinear FPSM is compared with the FEM and the traditional SD model in Fig. 10. The relative errors of the electromagnetic torque for the nonlinear FPSM and traditional SD model are 2.1% and 18.2%, respectively. The results predicted by the nonlinear FPSM match well with FEM results, but there are some errors in the traditional SD model because it cannot consider magnetic saturation. The cogging torque predicted by the nonlinear FPSM is also compared with FEM and traditional SD model in Fig. 11, and there is excellent agreement between these three waveforms because the machine has a low saturation level in this situation.

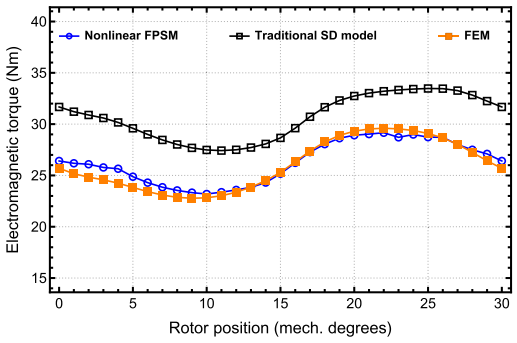

Fig. 10. Electromagnetic torque waveform.

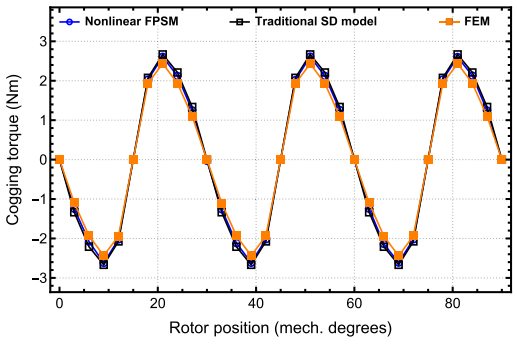

Fig. 11. Cogging torque waveform.

Both the FPSM and the FEM involve the resolution of a linear system. For a matrix of 2401 in size, the FPSM gives an average error of 2.43% in a torque cycle. For the FEM with a matrix of 2442 in size, the average error is 6.48%. Therefore, for this similar small matrix size, the FPSM gives less error.

V. Comparison of Two ISMs

Different ISMs can be used to update the relative permeability of the CPs. Those methods have different convergence speeds. Two of them, namely BM (Fig. 5) and RM (Fig. 12), are compared for their convergence speeds using the same NIA mentioned above. The range of coefficient α in the RM is from 0 to 1.

We randomly selected 500 machines for the studied SMPMM. We used two iterative methods to obtain the

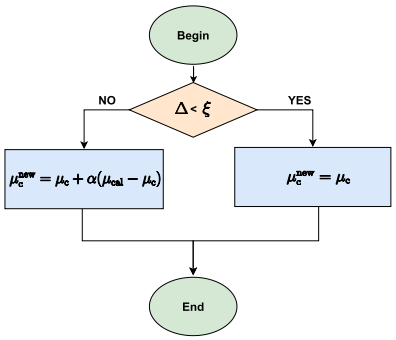

Fig. 12. RM.

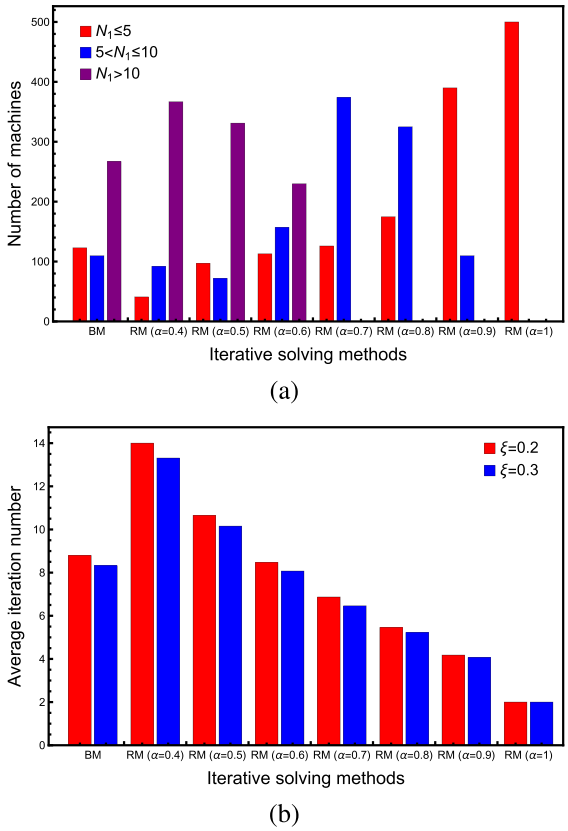

Fig. 13. Statistical analysis. (a) Distribution of the number of machines under different ISMs for $\xi = 0.2$ (N_1 represents the average iteration number for each machine). (b) Comparison of iteration numbers for different ISMs under two different allowable errors.

average number of iterations required to calculate several rotor positions within a torque cycle for each machine. There are 11 rotor positions selected in a torque cycle for calculation. Therefore, for each ISM, 5500 calculations are executed.

Fig. 13(a) shows the distribution of the number of machines under different ISMs. For the RM, most machines have less than ten iterations as α increases. For the BM, most machines need more than ten iterations, which requires more computation time than RM. Overall, the convergence speed of the RM is faster than BM when α is bigger or equal to 0.6.

The average iteration number of these results is taken as the reference value for convergence speed [Fig. 13(b)]. For the RM, as α increases, the iteration number required by the RM gradually decreases. Therefore, a larger α can speed up the computation for this optimization strategy. The BM needs more iterations than the RM when $\alpha > 0.6$, but the BM does not have a coefficient that needs to be determined. When $\alpha = 1$, the model of the SMPMM converges very quickly, in two iterations in our case, with the allowable error $\xi = 0.2$. The RM with $\alpha = 1$ is the best approach in our situation.

VI. Conclusion

This article presents an accurate multiobjective optimization strategy, which combines the nonlinear FPSM with the NSGA-II algorithm to find a Pareto front that helps design SMPMMs. The comparison results between this strategy and FEM for one optimal case confirm the effectiveness of the presented optimization strategy. Also, two different ISMs are compared for their convergence speed based on statistical analysis. The RM has a faster convergence speed than the BM when using $\alpha \geq 0.6$. With our type of SMPMM, the RM with $\alpha = 1$ is the best approach as it converges very quickly, in two iterations only.

Acknowledgment

This work was supported in part by the National Natural Science Foundation of China under Grant 52150610491, Grant 51837010, and Grant 51827810.

References

[1] P.-D. Pfister and Y. Perriard, "Slotless permanent-magnet machines: General analytical magnetic field calculation," *IEEE Trans. Magn.*, vol. 47, no. 6, pp. 1739–1752, Jun. 2011.

[2] P.-D. Pfister, X. Yin, and Y. Fang, "Slotted permanent-magnet machines: General analytical model of magnetic fields, torque, eddy currents, and permanent-magnet power losses including the diffusion effect," *IEEE Trans. Magn.*, vol. 52, no. 5, pp. 1–13, May 2016.

[3] L. Roubache, K. Boughrara, F. Dubas, and R. Ibtiouen, "New subdomain technique for electromagnetic performances calculation in radial-flux electrical machines considering finite soft-magnetic material permeability," *IEEE Trans. Magn.*, vol. 54, no. 4, pp. 1–15, Apr. 2018.

[4] Z. Djelloul-Khedda, K. Boughrara, F. Dubas, A. Kechroud, and B. Souleyman, "Semi-analytical magnetic field predicting in many structures of permanent-magnet synchronous machines considering the iron permeability," *IEEE Trans. Magn.*, vol. 54, no. 7, pp. 1–21, Jul. 2018.

[5] F. Cupertino, G. Pellegrino, and C. Gerada, "Design of synchronous reluctance motors with multiobjective optimization algorithms," *IEEE Trans. Ind. Appl.*, vol. 50, no. 6, pp. 3617–3627, Nov. 2014.

[6] X. Zhu, W. Wu, L. Quan, Z. Xiang, and W. Gu, "Design and multiobjective stratified optimization of a less-rare-earth hybrid permanent magnets motor with high torque density and low cost," *IEEE Trans. Energy Convers.*, vol. 34, no. 3, pp. 1178–1189, Sep. 2019.

[7] Y. Hua, H. Zhu, M. Gao, and Z. Ji, "Multiobjective optimization design of permanent magnet assisted bearingless synchronous reluctance motor using NSGA-II," *IEEE Trans. Ind. Electron.*, vol. 68, no. 11, pp. 10477–10487, Nov. 2021.

[8] H. Zhao, C. Liu, Z. Song, and W. Wang, "Exact modeling and multiobjective optimization of Vernier machines," *IEEE Trans. Ind. Electron.*, vol. 68, no. 12, pp. 11740–11751, Dec. 2021.

[9] C. Sun, Y. Fang, and P.-D. Pfister, "Comparison of two finite-permeability subdomain models for surface-mounted permanent-magnet machines," *IEEE Access*, vol. 11, pp. 73470–73477, 2023.

[10] C. Sun, Y. Fang, and P.-D. Pfister, "Torque calculation of surface-mounted permanent-magnet motors using subdomain model considering finite permeability: Influence of harmonic content," in *Proc. 26th Int. Conf. Electr. Mach. Syst. (ICEMS)*, Nov. 2023, pp. 3007–3011.